

# Optimal pupil size in the human eye for axial resolution

William J. Donnelly III and Austin Roorda

*University of Houston College of Optometry, 505 J. Davis Armistead Building, Houston, Texas 77204-2020*

Received January 29, 2003; revised manuscript received June 24, 2003; accepted July 2, 2003

A computer model that incorporates the monochromatic aberrations of the eye is used to determine the optimal pupil size for axial and lateral resolution as it applies to retinal imaging instruments such as the confocal scanning laser ophthalmoscope. The optimal pupil size for axial resolution, based on the aberrations of 15 subjects, is  $4.30 \text{ mm} \pm 1.19 \text{ mm}$  standard deviation (sd), which is larger than that for lateral resolution [ $2.46 \text{ mm} \pm 0.66 \text{ mm}$  (sd)]. When small confocal pinholes are used, the maximum detected light is obtained with a pupil size of  $4.90 \text{ mm} \pm 1.04 \text{ mm}$  sd. It is recommended to use larger pupil sizes in imaging applications where axial resolution is desired. © 2003 Optical Society of America

OCIS codes: 330.5370, 330.6130.

## 1. INTRODUCTION

Aberrations in the optical system of the eye counteract the improvements in resolution that one expects to obtain, according to diffraction theory, with increasing pupil size. This is well understood for lateral resolution in the human eye. The effect of aberrations in connection with pupil size was quantified first by Campbell and Green<sup>1</sup> and in a follow-up paper by Campbell and Gubisch,<sup>2</sup> who determined that the pupil size that offered the best lateral resolution was typically between 2 and 3 mm in diameter. Studies since that time have confirmed this finding.<sup>3-5</sup> What has not been studied on a theoretical level is the effect of wave aberrations on the axial resolution of the eye.

Axial resolution is an important concept for imaging modalities such as the scanning laser ophthalmoscope (SLO), a device that can be used to collect optical image slices of retinal tissue.<sup>6</sup> The thinness of the optical section is limited by the diffraction and aberrations of the eye. Choosing the pupil size that balances these two and offers the sharpest focused spot in the axial direction will provide the thinnest optical section.

Pupil size influences both axial and lateral resolution. As the pupil size increases, the optics of the human eye will obey diffraction theory and the axial resolution will increase, but only to a turning point. Beyond this point the blur due to high-order aberrations, introduced by the enlarging pupil, will reduce both axial and lateral resolution. This turning point yields the optimal pupil size for that individual. However, given that lateral resolution depends linearly on pupil size and axial resolution depends on the square of the pupil size, one cannot expect the turning point for optimal resolution to be the same for axial and lateral resolution. In this paper we show that the optimal pupil size for axial resolution is larger than the optimal pupil size for lateral resolution.

## 2. METHODS

### A. Axial Resolution

The metric chosen for axial resolution was relevant for the confocal SLO, an instrument that uses a focused light beam to obtain axial resolution. In an SLO with an optimally sized confocal pinhole, the effective point-spread function (PSF) is proportional to the square of the intensity of the three-dimensional (3D) point-spread function,<sup>7</sup> even when the eye has aberrations.<sup>8</sup> The squaring is a direct optical property of the confocal pinhole.<sup>9</sup> The result is that the confocal SLO measures only scattered light from features that are near the best focal plane. The axial resolution could be computed in a number of ways. For example, axial resolution could be described as the ability of an optical system to resolve two points separated in the *Z* direction. In this case, the axial resolution would be computed as the full width at half-maximum (FWHM) of a plot of the value of the squared PSF along the *Z* axis. We opt for a more conventional and meaningful metric for axial resolution, that of a planar object. If a diffuse-scattering planar surface is moved axially through the plane of best focus, the detected intensity at each position varies with the square of the integrated intensity of the changing PSF.<sup>9,10</sup> Whereas the integrated intensity for each axial position would be the same in all planes if the PSF were not squared (as is the case for a conventional imaging system), the squaring introduces a nonlinearity that enhances high-intensity peaks and attenuates the low-intensity regions.

3D PSFs were computed by use of a model eye that was generated with ZEMAX optical design software (Focus Software, Tucson, Ariz). The model eye was a reduced eye, with an index of refraction of 1.33 that had a perfect lens (diffraction-limited) with a secondary focal length (in the eye) of 20.2 mm. The length 20.2 was chosen because that is the distance from the exit pupil to the retina in the

Gullstrand eye model.<sup>11</sup> With this distance, the numerical aperture in the model eye was similar to that of a human eye. A consequence of using a reduced eye instead of an actual eye, however, is that in the reduced eye the entrance and exit pupils are the same, whereas in the actual eye the entrance pupil is 10.0% larger than the exit pupil (as computed from the Gullstrand eye model). To scale back into practical object space (i.e., entrance pupil) scales, we had to correct the pupil sizes. For example, to convert our optimal exit pupil sizes to their corresponding entrance pupil sizes, we had to multiply our pupil size values by 1.10.

A user-defined phase screen, defined by a Zernike polynomial function, was added to the model eye to generate known aberrations. We collected Zernike descriptions of the wave aberrations of the eyes of 16 subjects aged 20–35 yr. for our computer eye models. The research followed the tenets of the World Medical Association Declaration of Helsinki. Informed consent was obtained from the subjects after we explained the nature and possible complications of the study, and our experiments were approved by the University of Houston Committee for the Protection of Human Subjects. Aberrations were measured with a custom-built Shack–Hartmann wave-front sensor (400- $\mu\text{m}$  lenslets, 24-mm focal length) over a dilated pupil. The wave aberrations for a 6.6-mm subpupil centered in the dilated pupil were fitted with a 10th-order Zernike polynomial function. Each subject's aberrations were taken as the average of five repeated measures. Aberrations for smaller pupil sizes were determined by refitting a new wave-aberration function to subpupils that were centered and sampled from the original 6-mm wave-aberration function. The aberrations of each subject were corrected for sphere and astigmatism, to mimic the subject's best spectacle correction. ZEMAX automatically computed and stored digital images of the diffraction-based PSF for a range of image planes. For each eye, the 3D PSF was computed in 40 slices over a 2-mm axial section that spanned the plane of best focus. The wavelength chosen for all calculations was 632 nm. Each 3D PSF's envelope dimensions were 140  $\mu\text{m}$  ( $x$  width)  $\times$  140  $\mu\text{m}$  ( $y$  width)  $\times$  2000  $\mu\text{m}$  ( $z$  depth).

The integrated intensity of the squared PSF in each slice was plotted against its axial depth, and the axial resolution was defined as the FWHM of the resulting curve. The 40 points along the curve were interpolated, by use of a simple linear interpolation, to 200 points to facilitate measures of the FWHM. Figure 1 illustrates the procedure for calculating the axial resolution. Calculations were done for pupil sizes from either 1 mm or 2 mm to 6 mm in 0.25-mm steps. The optimal pupil size was selected as the one that gave the narrowest FWHM of the integrated intensity. A series of squared 3D PSFs for a typical subject is shown on Fig. 2, compared with the 3DPSFs for a diffraction-limited eye.

The Strehl ratio of the PSF was also plotted for the range of focal planes in the through-focus PSF. The Strehl ratio is defined as the ratio of the actual PSF maximum intensity to the diffraction-limited PSF intensity at optimal focus for the same pupil size. For comparison purposes and to illustrate the best possible situation, a diffraction-limited eye was included in the computation.

For each pupil size, the lateral resolution was also computed in the focal plane with the highest Strehl ratio. For the pupil sizes that provided the best lateral resolution, the focal plane that had the highest Strehl ratio generally coincided with the focal plane that provided the

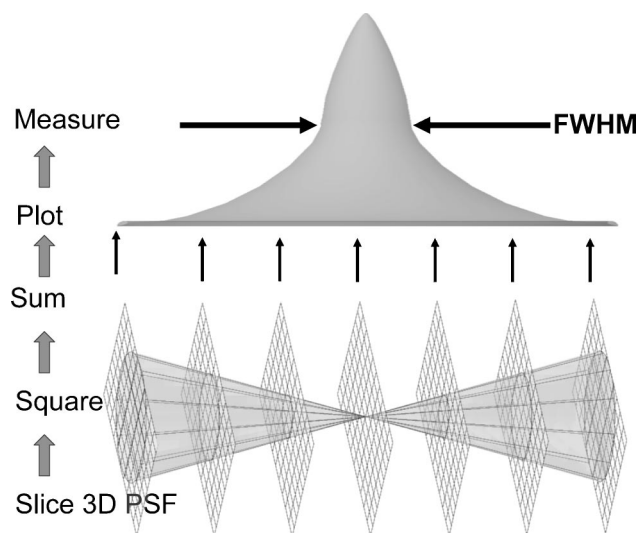


Fig. 1. Procedure for calculating axial resolution. First the 3D PSF is calculated as a sequence of 40 PSF images, with intensities relative to the diffraction-limited eye. Each value on each slice of the 3D PSF is squared, and then each slice is integrated and plotted against its axial position. The FWHM of the resulting function is computed to get the axial resolution.

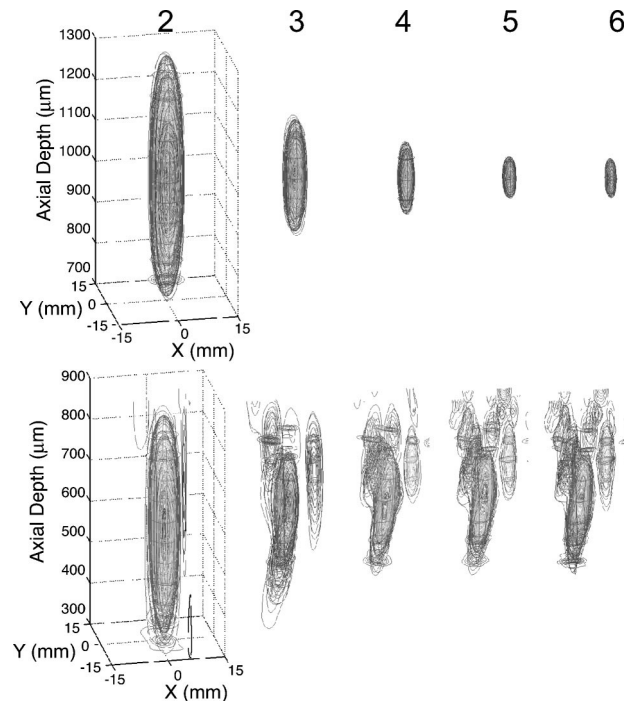


Fig. 2. 3D PSF with changing pupil size. The squared PSFs are shown here. In the diffraction-limited eye (upper series of PSFs), the squared 3D PSF becomes more compact, both laterally and axially. For a typical eye (lower series of PSFs), the squared 3D PSF looks similar to that in the diffraction-limited case for small pupils and starts to reduce in size with an increase in pupil size. After a certain point, aberrations begin to spread the PSF again.

**Table 1. Summary of Optimal Pupil Sizes for Axial Resolution, Lateral Resolution, and Maximum Detected Intensity**

Subject	For Best Axial Resolution			For Best Lateral Resolution			For Maximum Intensity Pupil (mm)
	Pupil (mm)	Ax. Res. ( $\mu\text{m}$ )	Lat. Res. ( $\mu\text{m}$ )	Pupil (mm)	Ax. Res. ( $\mu\text{m}$ )	Lat. Res. ( $\mu\text{m}$ )	
AV	3.30	215	9.4	2.75	253	7.4	3.58
AG	3.85	195	10.2	3.03	205	6.0	3.85
AR	3.30	195	6.8	3.03	205	6.4	3.30
BD	3.03	458	43.0	1.38	1571	16.8	5.78
BW	6.60	253	20.2	1.93	585	10.0	6.60
EM	4.13	214	12.4	3.03	263	7.6	4.13
EW	3.58	263	11.6	2.48	361	9.0	5.50
GQ	3.03	273	9.6	2.48	332	8.0	6.33
KD	4.95	244	14.4	2.48	419	9.6	4.68
KL	5.50	166	14.2	3.30	195	6.2	4.68
LW	5.50	244	12.8	2.48	409	8.4	5.23
LR	5.23	448	27.6	1.65	809	11.6	4.68
MR	2.48	361	10.0	2.20	410	8.8	3.58
SH	3.85	302	25.6	1.10	819	15.6	4.68
SN	4.68	166	10.6	3.30	195	6.4	6.05
TL	5.78	234	16.0	2.75	332	7.2	5.78
Avg.	4.30	264	15.9	2.46	460	9.1	4.90
SD	1.19	89	9.3	0.66	356	3.2	1.04

maximum detected intensity. The value for lateral resolution was computed as the diameter of the circle that contained 50% of the energy in the two-dimensional PSF for that plane. The optimal pupil for lateral resolution was selected as the one that had 50% of the encircled energy of the PSF within the smallest diameter.

### B. Scaling Integrated Intensity

The integrated intensity in the through-focus plots was scaled in such a way to account for the changing pupil area and its corresponding increase in detected light. This was done to allow for relative comparisons in detected light levels for different pupil sizes. For the model, the amount of light entering the eye was taken to be the same for all pupil sizes. The model was tested by confirming that the detected light levels for an eye with no aberrations showed an increase in detected light with increasing pupil size that was proportional to the square of the area of the pupil. The expected increase with pupil size arises for two reasons. First, an increase in intensity occurs because the amount of detected light increases linearly with the exit pupil area. Second, diffraction dictates that the light will be concentrated in the confocal aperture by the square of the area also (i.e., the irradiance in the Airy disk scales linearly with the pupil area). The pupil size that delivered the most light through the confocal pinhole aperture was determined for each subject; see Table 1. Directionality of the reflection due to the waveguiding properties of the photoreceptors<sup>12</sup> was not taken into account for this calculation.

## 3. RESULTS

### A. Axial Resolution

Charts were generated for each subject, showing the through-focus integrated intensities and the through-

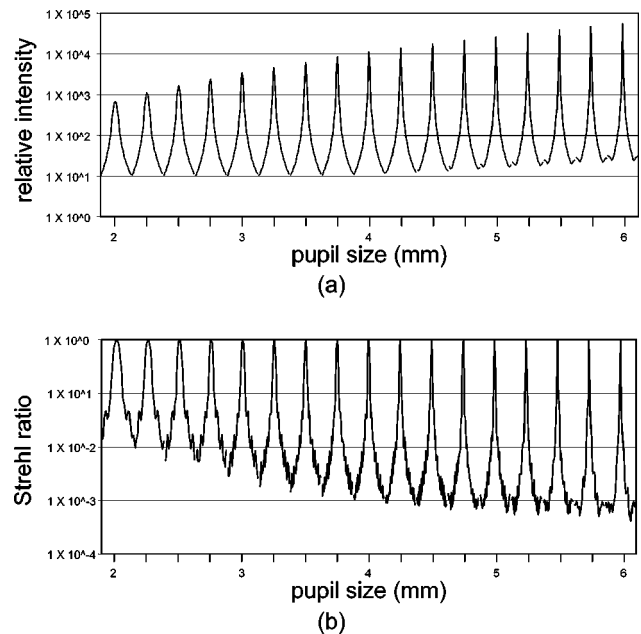


Fig. 3. (a) Integrated through-focus intensity of the 3D PSF as a function of axial location plotted for a diffraction-limited eye. Each curve segment shows one through-focus intensity plot over a 2-mm axial depth of the 3D PSF (the scale for each curve segment is not shown). The series of segments represent the individual plots for each pupil size. As expected, the detected intensity increases as the pupil size increases, and the width of the integrated intensity plots decreases as the pupil size increases. (b) Through-focus Strehl ratio as a function of axial location for a range of pupil sizes. The Strehl ratio is always equal to 1 at the best focal plane.

focus Strehl ratios as a function of pupil size. Example charts for a diffraction-limited eye and a typical subject are shown on Figs. 3 and 4. The integrated intensities

are in arbitrary units but are scaled relative to one another. Therefore the simulations also indicate the relative amount of detected light for each pupil size. The diffraction-limited eye (Fig. 3) shows expected results. There is an increase in the amount of detected light that scales with the square of the area of the exit pupil, and the Strehl ratio is always equal to 1 at the best focal plane. Figure 4 shows the results for a representative human subject. The FWHM narrows but only to a point after which it broadens again. Similarly, the intensity increases to a point but decreases again for large pupils.

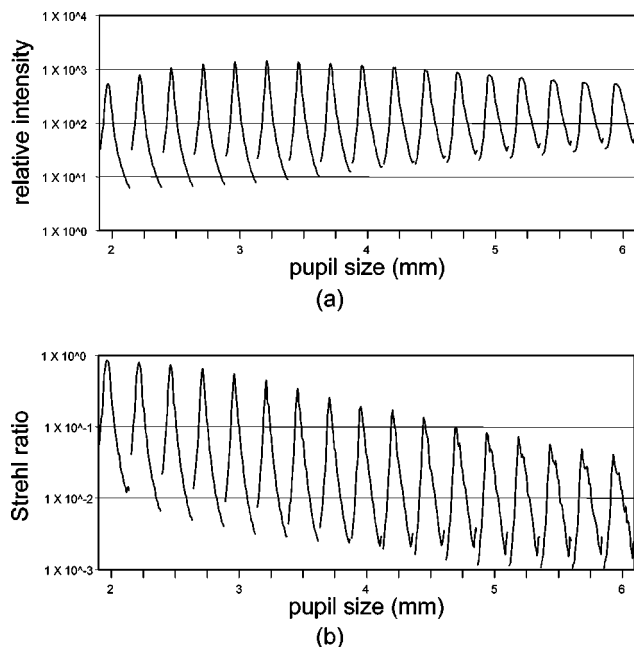


Fig. 4. (a) Integrated intensity of the 3D PSF as a function of axial location plotted for a typical eye (subject AV). The detected intensity increases to a point but then decreases as the pupil size increases. Similarly, the width of the integrated intensity plots narrows with increasing pupil size to a point ( $\sim 3$  mm) but then increases again as pupil size increases. Plots of the FWHM of these curves are shown in Fig. 5. (b) Through-focus Strehl ratio as a function of axial location for a diffraction-limited eye. The Strehl ratio is close to 1 for small pupils but decreases to  $\sim 0.05$  for a 6-mm pupil.

It is interesting to note that the presence of aberrations actually pulls light from the center of the PSF to the extent that the amount of detected light decreases for the large pupil sizes. The maximum Strehl ratio peaks near 1 for small pupils but reaches less than 5% for the largest pupil size.

From the data on these charts, we computed the FWHM of the integrated intensity curves and plotted the FWHM as a function of pupil size. The FWHM for each pupil diameter for every subject is plotted in Fig. 5. The lowest point on each curve indicates the best axial resolution for that subject. The corresponding pupil size at the best axial resolution corresponds to each subject's optimal pupil size for axial resolution.

## B. Lateral Resolution

The 50% encircled energy radius as a function of pupil size is shown for each subject on Fig. 6. We use the diameter of this circle to define the lateral resolution. The lowest point on each curve was the best lateral resolution for that subject, and the optimal pupil size for lateral resolution was the pupil size corresponding to this point.

## C. Comparison of Axial and Lateral Resolution

Results are listed in Table 1. Each subject's best axial and lateral resolutions are listed with their corresponding pupils.

## 4. DISCUSSION

### A. Pupil Size Differences for Axial and Lateral Resolution

The average pupil sizes for best lateral and axial resolution are significantly different from each other (see Table 1). Axial resolutions are best with larger pupils, averaging  $4.30 \pm 1.19$  mm. Lateral resolutions are best with smaller pupils, averaging  $2.46 \pm 0.66$  mm, consistent with other literature on lateral resolution.<sup>1</sup> For all but one case (axial resolution for subject BW) axial resolution shows a local minimum (Fig. 5). There is also a great deal of variability between the subjects, especially for axial resolution.

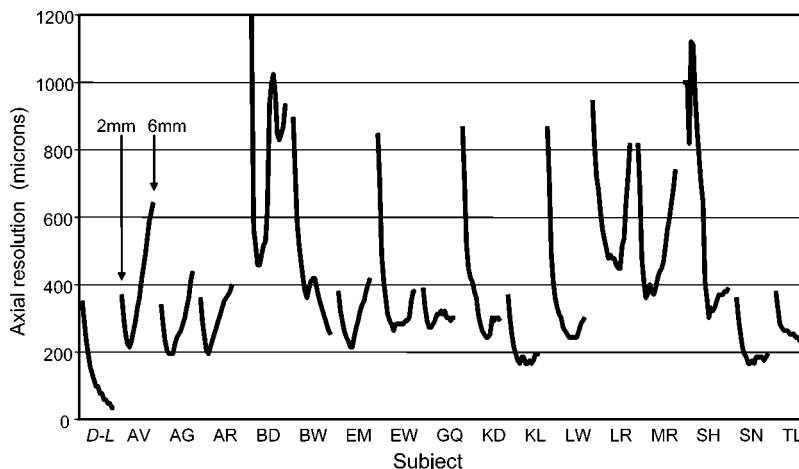


Fig. 5. Plots of axial resolution versus pupil diameter. All subjects are shown here including the diffraction-limited eye, labeled *D-L*. For all cases but one (subject BW), the axial resolution reached a minimum for a pupil size between 2 and 6 mm.

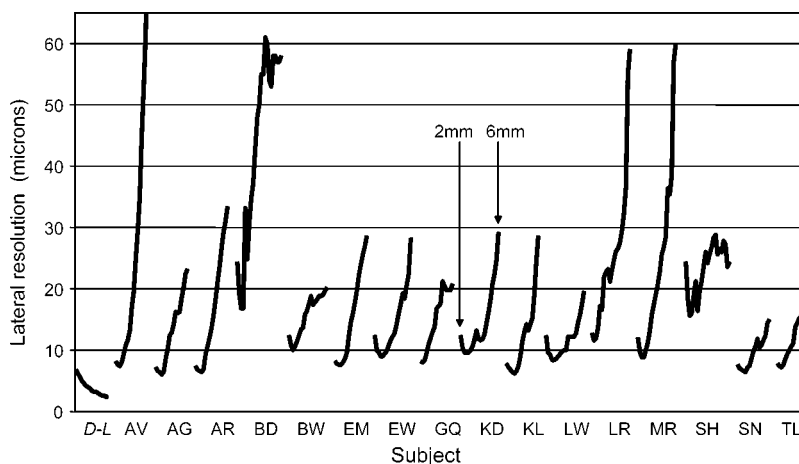


Fig. 6. Plots of lateral resolution (50% encircled energy) versus pupil diameter. All subjects are shown here including the diffraction-limited eye, labeled *D-L*. For all cases, the lateral resolution reaches a minimum for a pupil size between 2 and 6 mm.

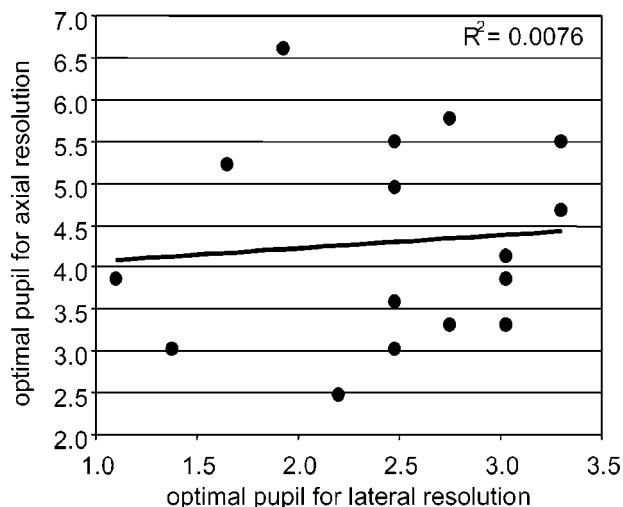


Fig. 7. Comparison of best pupil for axial resolution versus best pupil for lateral resolution. The correlation between the two numbers is very low, indicating that if the pupil size for best lateral resolution is known, it is not possible to predict the best pupil for axial resolution.

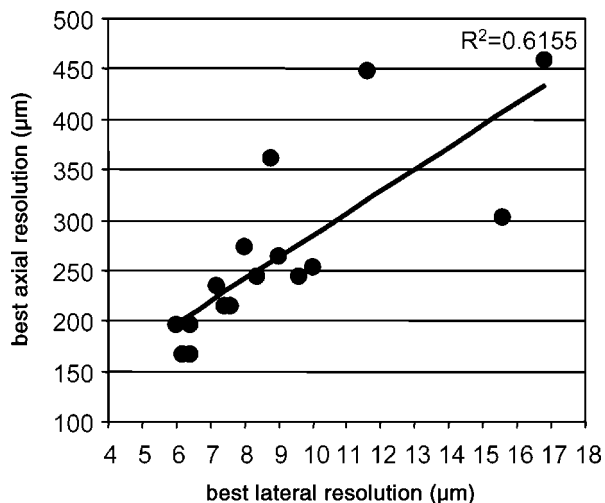


Fig. 8. Comparison of best axial resolution versus best lateral resolution. This plot indicates that improving the lateral resolution will also increase the axial resolution.

**B. Intensity**

The calculations (see Table 1) show that in an SLO, more light can be collected through a pupil that is smaller than the maximum, even if the same amount of incident light is used. Even though more light emerges from a larger pupil, the associated aberrations serve to pull information out of the core of the 3D PSF, limiting not only the axial resolution but also the absolute amount of light than can be detected through the confocal pinhole. As seen in Fig. 4, the integrated intensity plots show a peak detected intensity for an intermediate pupil size. The pupil size for maximum intensity is, on average, 14% larger than the pupil size for best axial resolution.

**C. Correlation between Lateral and Axial Resolution**

From theory, the axial resolution for a diffraction-limited eye is predicted to improve with the square of the lateral resolution as the pupil size increases.<sup>10</sup> This relationship also holds when the aberrations are small. For example, we find a quadratic relationship ( $R^2 = 0.8946$ ) between the axial and the lateral resolution when they are plotted for the pupil sizes that give the best lateral resolution. These pupils are relatively small (average size 2.46 mm), and the aberrations are low. However, similar relationships do not persist when significant aberrations are present. Considerable complexity in the 3D PSF and variability between individuals make it impossible to predict confidently any meaningful axial resolution metrics based on lateral resolution performance.

The most valuable correlation would be one that could predict the optimal pupil size for axial resolution once the optimal pupil size for lateral resolution is known. Figure 7 shows that this correlation is not possible. Another valuable prediction would be to determine how the potential axial resolution increases with increasing lateral resolution. Figure 8 shows that a linear regression can explain 61% of the variance. All the other correlations that might prove useful are not strong.

**D. Applications for Imaging**

The results in Table 1 show that if one selects the optimal pupil size for lateral resolution, then axial resolution will

be 74% worse than if the optimal pupil size for axial resolution is used (4,60 versus 26,4). Similarly, a 75% drop in lateral resolution can be expected if the optimal pupil size for axial resolution is used (15.9  $\mu\text{m}$  versus 9.1  $\mu\text{m}$ ). For overall optimal imaging performance, one might opt for a pupil size that is midway between the two.

Our model used a common pupil size for light illumination and light detection, as well as an infinitely small pinhole. This is generally not the way that current commercially available SLOs operate. Had we modeled a small, fixed illumination aperture, then we would have obtained a similar result, although the changes in resolution and intensity as a function of pupil size would have been less dynamic. When a larger confocal pinhole is used, it de-emphasizes the importance of good resolution on the return path, and in such cases it is advisable to use an optimal illumination pupil for lateral resolution and a large detection pupil. It follows that with a large confocal pinhole, the amount of detected light would be maximal for the largest collection pupil. It also follows that under such conditions, the axial resolution would be compromised.

## 5. CONCLUSIONS

The optimal pupil size for axial resolution is larger than for lateral resolution. This is not surprising since diffraction theory states that axial resolution increases with the square of the pupil size, whereas the lateral resolution increases linearly. It follows that the pupil size that balances the effects of diffraction and aberration will not be the same in the two cases.

Because the optimal pupil sizes are different, a different pupil size may be selected for imaging depending on whether the results demand better axial or better lateral resolution. Since there are a lot of interindividual differences in the optimal pupil sizes for both lateral and axial resolution, it would be best to select the optimal pupil size on the basis of the aberrations of each individual eye. Given ever-increasing computing power, better eye models, and a better understanding of the eye's optics, using a custom pupil size for each eye is not unreasonable.

A step toward acquiring the best possible images of the retina is to use the optimal pupil for the desired resolution application. However, even with an optimal pupil size, the aberrations that are present in the eye worsen

both axial and lateral resolution. If these aberrations can be corrected, such as with adaptive optics, better axial and lateral images of the retina can be obtained with larger pupils.

## ACKNOWLEDGMENTS

This research was funded in part by the National Science Foundation, Science and Technology Center for Adaptive Optics, managed by the University of California at Santa Cruz under cooperative agreement AST 9876783.

The authors may be reached by e-mail as follows: Austin Roorda, aroorda@uh.edu; William J. Donnelly III, Wdonnelly.2001@alumni.opt.uh.edu.

## REFERENCES

1. F. W. Campbell and D. G. Green, "Optical and retinal factors affecting visual resolution," *J. Physiol.* **181**, 576–593 (1965).
2. F. W. Campbell and R. W. Gubisch, "Optical quality of the human eye," *J. Physiol.* **186**, 558–578 (1966).
3. H. C. Howland and B. Howland, "A subjective method for the measurement of monochromatic aberrations of the eye," *J. Opt. Soc. Am.* **67**, 1508–1518 (1977).
4. G. Walsh, W. N. Charman, and H. C. Howland, "Objective technique for the determination of monochromatic aberrations of the human eye," *J. Opt. Soc. Am. A* **1**, 987–992 (1984).
5. J. Liang and D. R. Williams, "Aberrations and retinal image quality of the normal human eye," *J. Opt. Soc. Am. A* **14**, 2873–2883 (1997).
6. R. H. Webb, G. W. Hughes, and F. C. Delori, "Confocal scanning laser ophthalmoscope," *Appl. Opt.* **26**, 1492–1499 (1987).
7. T. Wilson and C. J. R. Sheppard, *Theory and Practice of Scanning Optical Microscopy* (Academic, London, 1984).
8. A. Roorda, "Double pass reflections in the human eye," Ph.D. thesis (University of Waterloo, Waterloo, Ontario, Canada, 1996).
9. T. Wilson, "The role of the pinhole in confocal imaging systems," in *The Handbook of Biological Confocal Microscopy*, J. B. Pawley, ed. (Plenum, New York, 1990), pp. 99–113.
10. A. W. Dreher, J. F. Bille, and R. N. Weinreb, "Active optical depth resolution improvement of the laser tomographic scanner," *Appl. Opt.* **28**, 804–808 (1989).
11. A. G. Bennett and R. B. Rabbetts, *Clinical Visual Optics*, 2 (Butterworth, London, 1989).
12. G. J. van Blokland, "Directionality and alignment of the foveal receptors, assessed with light scattered from the human fundus *in vivo*," *Vision Res.* **26**, 495–500 (1986).